IN SITU WATER DISTRIBUTION MEASUREMENTS IN AN OPERATING POLYMER ELECTROLYTE FUEL CELL

M. M. Mench[1,2], Q. L. Dong, and C. Y. Wang[1]
Electrochemical Engine Center, and
Department of Mechanical and Nuclear Engineering
The Pennsylvania State University
University Park, PA 16802

ABSTRACT

The water balance between the flow channels, gas diffusion layer, and electrolyte membrane is a critical phenomenon affecting polymer electrolyte fuel cell (PEFC) performance. This paper presents data on the *in situ* water distribution within the gas channel of an operating PEFC. Following careful calibration and instrumentation, a gas chromatograph (GC) was interfaced directly to the fuel cell at various locations along the serpentine anode and cathode flow paths of a specially designed fuel cell. The 50 cm^2 active area instrumented fuel cell also permits simultaneous current distribution measurements via the segmented collector plate approach. The on-line GC method allows discrete measurements of the water vapor content of the flow about every two minutes. Water distribution data are shown at several inlet relative humidities and cell operating voltages. For the thin electrolyte membranes used (51 μm), there is little functional dependence of anode gas channel water distribution on current output. For thin membranes, this indicates that there is little gradient in the water activity between anode and cathode, for the conditions tested ($i < 1$ A/cm^2).

---

[1] Electrochemical Society Active Member
[2] Author to whom correspondence should be addressed: e-mail mmm124@psu.edu; Phone: (814) 865-0060; Fax: (814) 863-4848

INTRODUCTION

The hydrogen polymer electrolyte fuel cell (PEFC) has tremendous promise as a future power system due to its low pollution, high efficiency, and stealth. Many studies, too numerous to completely list, have examined various aspects of PEFC performance as a function of operating conditions (1-9). Gottesfeld wrote an excellent review of PEFC components and operation, and the reader is referred to it for additional information on PEFC fundamentals (10). In addition to experimental characterization, much research has been focused on first-principles based modeling of the PEFC system (11-21). However, advances in modeling of the PEFC have thus far outpaced the ability to experimentally verify the predicted performance. In particular, scant experimental data are presently available regarding current density and species distributions. As indicated by Wang (22), it is this type of detailed validation that will permit an ultimate understanding of the physicochemical phenomena in the PEFC as well as development of useful computer-aided tools for design and development.

Determination of the mass distribution is critical to understanding water management and reactant distribution effects. In particular, it is desirable to understand the water vapor distribution within the gas channels of the flowfield. Many authors have conducted detailed studies or deduced models that describe the water transport through fuel cell components including the electrolyte and porous gas diffusion layers (23-30). In order to integrate these models and validate their accuracy, it is desired to determine the *in situ* mole fraction distribution of water vapor, at various locations within the gas channel flow path. A few authors have completed detailed studies of the water balance in an operating cell by collection of the fuel cell effluent, and condensation of the gas-phase water vapor (31-34). While useful, these studies do not provide data on the water distribution throughout the cell, which could vary widely depending on operating conditions, current distribution, and local non-isotropic transport parameters. In order to delineate the effects of current distribution on water distribution, it is also desirable to couple water and current distribution measurements to provide detailed information on non-uniform transport and generation effects. The instrumented cell used in this study allows for simultaneous measurement of current and mass distribution.

As has been discussed by Mench and Wang (35,36), several authors have developed different methodologies for current density distribution (37-41). The instrumented cell utilized in this work utilizes gold plated, segmented current collector similar to that described by Mench and Wang (35,36). The reader is referred to these papers for more detail on this methodology for current distribution measurements using a non-segmented MEA. This paper is concerned solely with mass distribution measurement technique.

EXPERIMENTAL

Instrumented Cell Design

Specific details and geometry of the instrumented cell and segmented flowfield are given in Finckh (42). The flowfield of the anode and cathode is a single-pass serpentine flowfield. Figure 1 is a schematic diagram detailing the relevant dimensions of the fuel cell. The dimension of the flow channel was chosen to be 2.16 mm wide, 3.18 mm in depth and had an average pass length of approximately 71 mm. With a total of 22 serpentine passes, the total path length is 1577 mm. Teflon® gaskets were press fit over the protruding gold-plated rib landings to form a flush surface with the polycarbonate slab. Two additional sealing gaskets surrounded both gas diffusion layers (GDL) of the MEA to compensate for GDL thickness. Gold plating, and use of an optimized compression torque for the cell of 35 in-lbs minimized electrical contact resistance between rib landings and the GDL. Pressure indicating film (Pressurex® by Sensor Products, Inc.) was used to determine the *in-situ* pressure distribution of the landings onto the MEA, as a function of compression torque. The assembly was checked to ensure a homogeneous pressure distribution from all landings onto the gas diffusion layer, thus ensuring a uniform contact resistance distribution between the gold-plated landings and GDL. The entire fuel cell assembly was leak proof tested to 0.3 MPa under water.

A schematic of the test and control system is shown in Fig. 2. Ultra-high purity (>99.999%) hydrogen and standard compressed air were supplied from compressed gas-cylinders. A steam-injection humidifier system (Lynntech Inc.) was used to provide the desired humidification to anode and cathode flows through control of the precise amount of water vapor added to the gas streams. Between humidifier and fuel cell, electric heating tapes were wrapped around the pipes to eliminate any condensation. Directly upstream of the inlet to the fuel cell, a gas sampling port was installed to measure the input humidity to the fuel cell by an Agilent 3000 MicroGC. This port was in addition to those along the fuel cell anode and cathode flow paths and provided accurate measurement and control of the humidification entering the cell.

The fuel cell system, including all lines leading to the fuel cell, were heated to the desired temperature, which was maintained with several Omega Engineering, Inc. model 8500 PID controllers. The cell and input lines maintained a steady temperature after suitable time to eliminate thermal transients. This start-up time was determined to be about ninety minutes by system check-out tests using thermocouples affixed to the GDL under non-flowing conditions.

To control and measure accurate current/voltage polarization curves, the fuel cell was connected to a multi-channel potentiostat/galvanostat (Arbin Instruments). For current density measurements, a gold-plated, electrically segmented current collector is used in direct contact with the unaltered GDL on the anode and cathode. In this segmented current collector technique, the potentiostat system maintains a constant voltage and the current sensors measure amperage emerging from each segmented current collector location, without the need for shunt resistors.

The membrane electrode assemblies (MEA) used for testing consisted of Nafion^{TM} 112 as the polymeric membrane, sandwiched between the catalyst and ELAT™ (E-Tek, inc.) carbon cloth diffusion layers. All MEAs used had a carbon-supported catalyst loading of 0.5 mg Pt/cm^2 on both anode and cathode. Other general operating conditions are given in Table 1.

For mass distribution measurements, eight species extraction ports are located within the 1st (4.3% *of the fractional distance along the single serpentine path from the channel inlet*), 4th (17.4%), 7th (30.4%), 10th (43.5%), 13th (56.5%), 16th (69.6%), 19th (82.6%) and 22nd (95.7%) reactant channel passes. The extraction takes place along the back wall of the polycarbonate plate, at the farthest distance from the MEA to reduce water droplet blockage and false readings. The fittings on the backing plates used for species extraction were Teflon™ to eliminate corrosion.

RESULTS AND DISCUSSION

Micro GC Calibration and Measurement

In order to accurately measure the hydrogen, oxygen, nitrogen, and water species present in the fuel cell, an Agilent 3000 MicroGC (GC) was utilized. Two GC columns were used for gas species separation, a Plot-U column, and a molecular sieve (Molsieve) column with backflush module for prevention of excess water damage. This type of GC is capable of performing a single measurement about every two minutes. The column temperature was set to 120°C to avoid water condensation, and carrier gases of UHP helium, a 7.5% H$_2$ balance helium, or argon were used. The GC was interfaced to the fuel cell through a 0.318 cm (0.125 in.) stainless steel, heated tube connected to the sample ports of the cell.   The sample line temperature was monitored and kept well above 100°C. Since reduced pressure flow can hold a greater mole fraction of water than pressurized flow, there is no condensation resulting from the pressure drop from the fuel cell channel to the GC inlet. The flow is directed toward the GC inlet and a bypass valve that allows continuous flow of atmospheric pressure sample gas. Sample availability at atmospheric pressure eliminates any error associated with varying sample inlet pressure, which can greatly affect results. The bypass flow was measured continuously with a mass flow meter to ensure that the extracted sample was a small fraction of the total fuel cell reactant flow. Typical values of bypass were 2-3% of the total flow, and this value never exceeded 5% during measurement. The possible disruption of performance by sample gathering on various channels was examined and determined to be minimal. Figure 3 shows continuous performance measurements between 0.4, 0.6, and 0.8 V at many locations along the anode path. During this continuous measurement, the sample extraction line was removed and replaced at several different locations, and many samples were taken. It is clear from this figure that no significant performance change results from withdrawal of such a small fraction of total flow from the channel.   In addition, the reproducibility of the current distribution results over long time scales and through voltage cycling is demonstrated with Figure 3.

Depending on the pressure of the fuel cell, the delivery time for species to go from the fuel cell to the GC varied from seconds to minutes, based on calculations of interior tube volume and known flow rate. All GC measurements were given adequate

time to ensure ample tube purge had occurred, and several measurements were taken to ensure accurate measurement.

In typical GC measurement applications, water vapor is condensed from the flow before entering the GC device. This is to prevent damage or degradation to the columns and detector elements. Indeed, if liquid water reaches the inlet of the GC or condenses inside the detector, system failure will likely occur. However, all temperatures of the columns, inlets, and sample tubes are kept well above $100^{o}C$ to prevent this. Because of the high amounts of water present and resultant accelerated deactivation of the separation columns, a backflush module was installed to block vapor flow into the molsieve column, and frequent GC column cleaning was conducted. Provided that all flow is maintained well above the dew point, very accurate and repeatable measurement of water content up to 90% mole fraction can be achieved.

Sample calibration: Calibration is required before every set of test runs to maintain accuracy of measurement. Calibration is accomplished with a gas-bubbler humidifier at low flow rate and controlled temperature as a standard to ensure a known exit humidity of the calibration gas mixture. Pressure is monitored at the humidifier exit to correct for any losses in the sample line. To complete calibration, a single point calibration is made at a low temperature of around $50^{o}C$, to correlate the measured response area to the thermodynamically known water vapor mole fraction. Then, the temperature of the humidifier is increased and the calibration correlation is not altered, but the output is checked against the theoretical value to ensure accuracy. The results are very consistent. The measured mole fraction is typically within ±2% of the theoretical value, up to very high values of water mole fraction up to $95^{o}C$. Calibration curves taken for fully humidified hydrogen and fully humidified air flow are shown in Figs. 4 and 5. The data shown represent an average of five measurements, and it can be seen that the expected accuracy is around ± 2%. Note the close agreement between the measured values of water fraction compared to the thermodynamically expected values, which change very steeply with temperature in the range of fuel cell operation. This calibration also indicates that the humidifier is near 100% humidification efficiency. Due to the steepness of the theoretical water vapor mole fraction curve, if the humidifier were significantly less than 100% efficient, the measured calibration curve would not follow the rapidly changing slope of the theoretical curve.

Anode inlet humidity variation: Figure 6 shows the measured water mole fraction at various locations within the anode flow channel for three fuel cell voltages. The current distribution associated with these measurements is shown in Fig. 3. The fuel cell exit pressure was ambient, with 100% humidification at $80^{o}C$ on the air cathode, and either 100% or 0% RH at $65^{o}C$ on the anode. Each data point shown represents an average of at least five data points. There was very little scatter in the data. This series of tests were designed to illustrate the following:

1) The uptake of water into the gas channel from dry inlet conditions in the anode.
2) The effect of current density (and thus changing electro-osmotic drag of water through the PEFC) on anode gas channel humidity ratio.

It can be seen from Fig. 6, that for both cases of different inlet humidity ratio, the water uptake follows an exponential approach to an asymptotic value that is greater than the thermodynamically allowed maximum at 80°C. One explanation for increased water content is that the cell temperature could be slightly higher than the prescribed 80°C. It should be noted that the inlet gas temperature to the anode was 90°C. In addition, the thermal contact resistance between the control thermocouple and the polycarbonate backing plate was demonstrated to be responsible for a one-degree difference between measured and true polycarbonate temperature. A one-degree temperature difference would account for a 5% change in the maximum theoretical mole fraction, within the limits of measurement. Another explanation for the increased water mole fraction beyond thermodynamic limit at 80°C is the possibility of entrained mist flow. It is difficult to gauge the latter, as experimental correlations do not publicly exist for the specific geometry of the fuel cell flowfield.

It can also be seen from Figure 6, that in most cases, the measured anode channel water content was not affected to a great degree by the voltage (and hence current) draw. In most cases, the highest current output (lowest cell voltage) condition resulted in the lowest measured anode channel water vapor content, although not to any significant degree. This strongly indicates that the electro-osmotic drag of water from the anode to the cathode is nearly evenly balanced by back diffusion. This is expected for very thin membranes, such as the 51 μm Nafion PEFC used for testing. This near balance of drag and diffusion of water with thin membranes has been observed experimentally by water condensation and collection techniques as well (32).

CONCLUSIONS

Gas chromatography has been used to measure the *in situ* flow channel water vapor distribution of an operating, specially instrumented fuel cell flow field. Additionally, the fuel cell used permits simultaneous current density distribution measurements. This technique can be used to directly map water distribution in the anode and cathode of an operating fuel cell with a time resolution of approximately two minutes, and a spatial resolution limited only by the closeness of sample extraction ports located in the reactant gas channels. Along with other diagnostic techniques such as current distribution mapping, this species mapping technique provides an important tool to understand water management and reactant distribution in PEFC. The anode channel water distribution was not greatly influenced by the current density. For the thin (51 μm) membranes used, the electro-osmotic drag of water from the anode to the cathode is nearly evenly balanced by back diffusion.
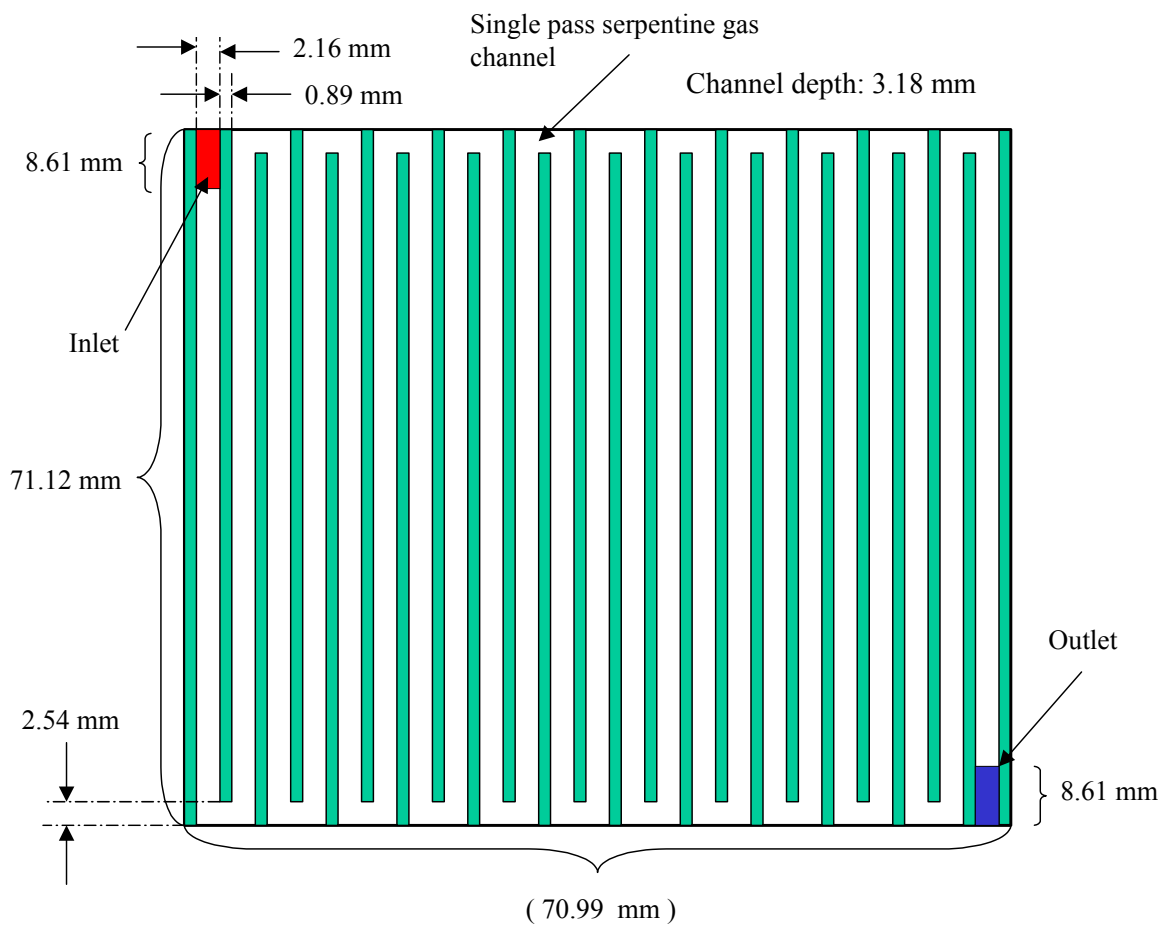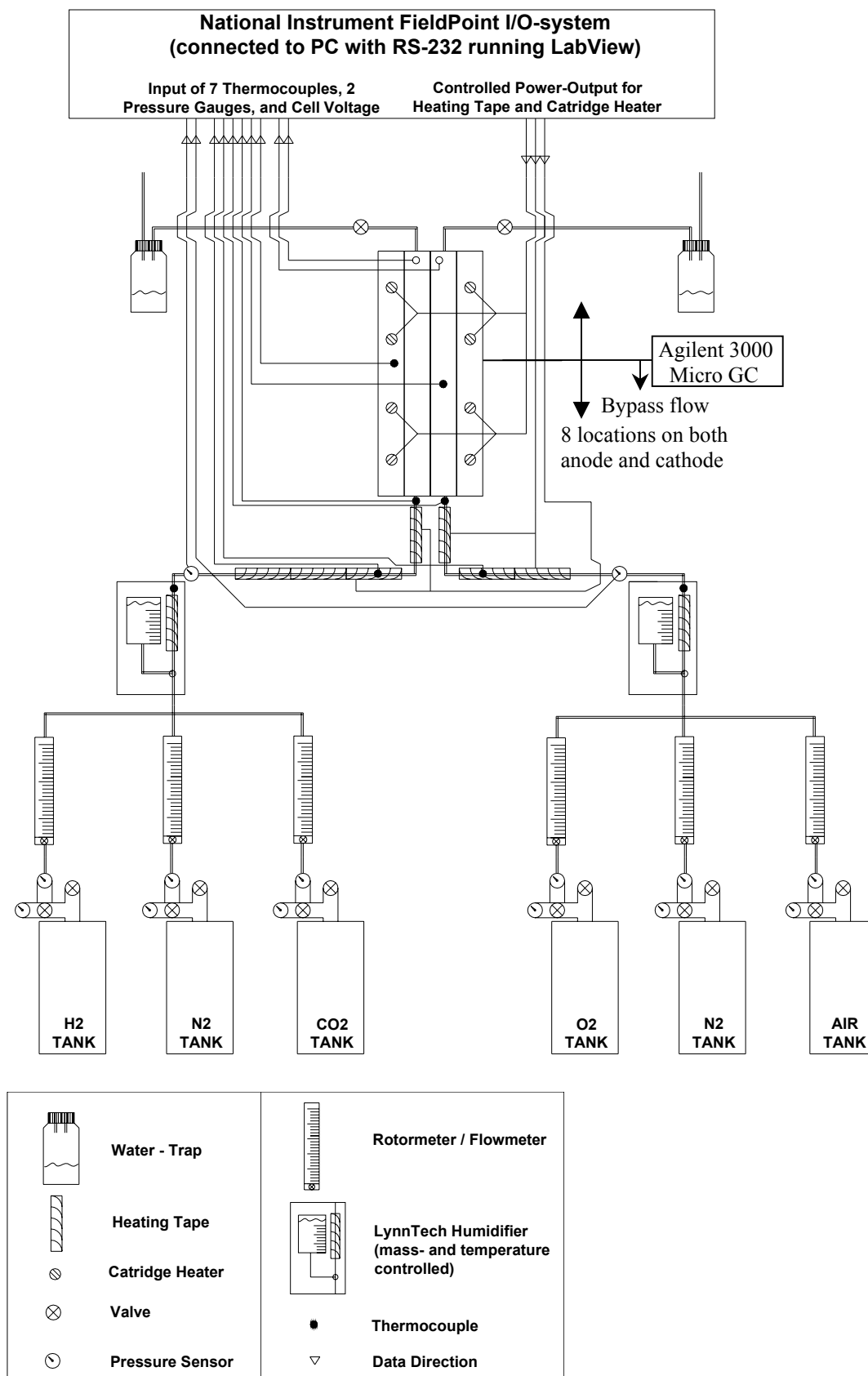
ACKNOWLEDGEMENTS

REFERENCES

1. A. Parthasarathy, S. Srinivasan, and A. J. Appleby, and C. Martin, *J. Electrochem. Soc.*, **139**, 2530 (1992).
2. A. Parthasarathy, S. Srinivasan, A. J. Appleby, and C. Martin, *J. Electrochem. Soc.*, **139,** 2856 (1992).
3. Y. W. Rho, O. A. Velev, S. Srinivasan, and Y. T. Kho, *J. Electrochem. Soc.*, **141**, 3838 (1994).
4. J. C. Amphlett, R. M. Baumert, R. F. Mann, B. A. Peppley, P. R. Roberge, and T. J. Harris, *J. Electrochem. Soc.*, **142**, 9 (1995).
5. R. Mosdale, and S. Srinivasan, *Electrochim. Acta*, **40**, 413 (1995).
6. H. –F. Oetjen, V. M. Schmidt, U. Stimming, and F. Trila, *J. Electrochem. Soc.*, **143**, 3838 (1996).
7. F. N. Büchi, and D. Srinivasan, *J. Electrochem. Soc.*, **144**, 2767 (1997).
8. F. A. Uribe, S. Gottesfeld, and T. A. Zawodzinski, *J. Electrochem. Soc.*, **149**, A293 (2002).
9. E. A. Ticianelli, C. R. Derouin, and S. Srinivasan, *J. Electroanal. Chem.,* **251**, 275 (1988).
10. S. Gottesfeld, in Advances in Electrochemical Science and Engineering, C. Tobias, Editor, **Vol. 5**, Wiley and Sons, New York (1997).
11. T. E. Springer, T. A. Zawodinski, and S. Gottesfeld, *J. Electrochem. Soc.*, **138**, 2334 (1991).
12. D. M. Bernardi and M. W. Verbrugge, *AIChE J.,* **37**, 1151 (1991).
13. D. M. Bernardi, and M. W. Verbrugge, *J. Electrochem. Soc.*, **139**, 2477 (1992).
14. T. E. Springer, M. S. Wilson, and S. Gottesfeld, *J. Electrochem. Soc.*, **140**, 3513 (1993).
15. T. V. Nguyen and R. E. White, *J. Electrochem. Soc.*, **140**, 2178 (1993).
16. C.Y. Wang and W.B. Gu, *J. Electrochem. Soc.*, **145,** 3407 (1998).
17. V. Gurau, H. Liu, and S. Kakac, *AIChE J.,* **44**, 2410 (1998).
18. J. S. Yi and T. V. Nguyen, *J. Electrochem. Soc.*, **146**, 38 (1999).
19. S. Um, C. Y. Wang and K. S. Chen, *J. Electrochem. Soc.*, **147**, 4485 (2000).
20. Z. H. Wang, C. Y. Wang and K. S. Chen, *J. Power Sources*, **94**, 40 (2001).
21. C. Y. Wang, S. Um, H. Meng, U. Pasaogullari, and Y. Wang, "Computational fuel cell dynamics (CFCD) models," *in 2002 Fuel Cell Seminar*, Nov. (2002).
22. C. Y. Wang, "Two-phase flow and transport in PEM fuel cells," *in Handbook of Fuel Cells*, John Wiley and Sons, (2002).
23. D. M. Bernardi, *J. Electrochem. Soc.*, **137**, 3344 (1990).
24. T. E. Springer, T. A. Zawodzinski, and S. Gottesfeld, *J. Electrochem. Soc.*, **138**, 2334 (1991).
25. D. M. Bernardi and M. W. Verbrugge, *J. Electrochem. Soc.*, **139**, 2477 (1992).
26. T. F. Fuller and J. Newman*, J. Electrochem. Soc.*, **140**, 1218 (1993).
27. M. Eikerling, Y. I. Kharkats, A. A. Kornyshev, and Y. M. Volfkovich, *J. Electrochem. Soc.*, **145**, 2684 (1999).
28. J. S. Yi and T. V. Nguyen, *J. Electrochem. Soc.*, **146**, 38 (1999).
29. I-M. Hsing, and P. Futerko, *Chem. Eng. Sci.*, **55**, 4209 (2000).
30. Z.H. Wang, C. Y. Wang and K. S. Chen, *J. Power Sources*, **94,** 40 (2001).
31. X. Ren and S. Gottesfeld, *J. Electrochem. Soc.*, **148**, A87 (2001).
32. G. J. Janssen, *J. Electrochem. Soc.*, **148**, A1313 (2001).
33. G. J. Janssen, M.L. Overvelde, *J. Power Sources*, **101**, 117 (2001).
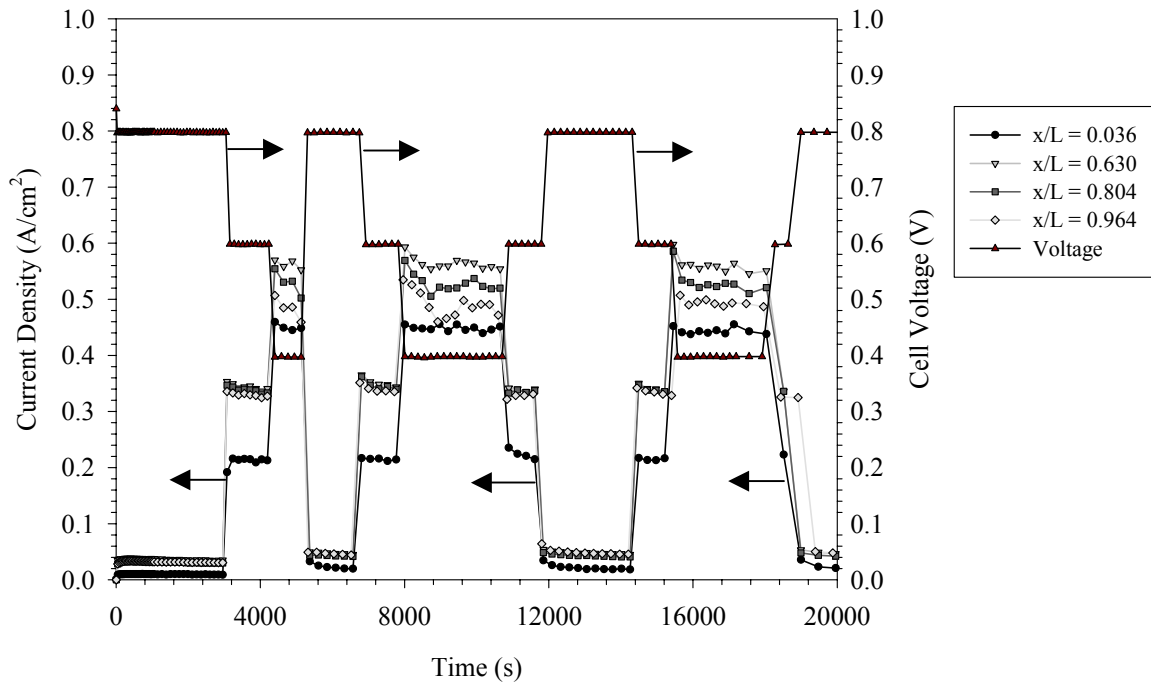
34. W.K. Lee, J. W. Van Zee, S. Shimpalee, and S. Dutta, *Proceedings of ASME Heat Transfer Division*, **1**, 339 (1999).
35. M. Mench, and C.Y. Wang, *J. Electrochem. Soc.*, **150,** A79 (2003).
36. M. Mench, C. Y. Wang, and M. Ishikawa, *Proceedings of the 202nd Meeting of the ECS,* ECS-S1-0814 (2002).
37. C. Wieser, A. Helmbold, and E. Gülzow, *J. of Appl. Electrochem.*, **30**, 803 (2000).
38. J. Stumper, S. Campell, D. Wilkinson, M. Johnson, and M. Davis, *Electrochim. Acta*, **43**, 3773 (1998).
39. S. Cleghorn, C. Derouin, M. Wilson, and S. Gottesfeld, *J. of Appl. Electrochem.*, **28**, 663 (1998).
40. M. Noponen, T. Mennola, M. Mikkola, T. Hottinen, and P. Lund, *J. Power Sources*, **106**, 304 (2002).
41. D. Brett, S. Atkins, N. Brandon, V. Vesovic, N. Vasileiadis, and A. Kucernak, *Electrochem. Comm.* 3, 628 (2001).
42. O. H. Finckh, "Dilution effects and current distribution on hydrogen proton exchange membrane fuel cells," MS Thesis, *The Pennsylvania State University*, May 2002.

Figure 1. Schematic diagram of the 50 cm^2 instrumented test cell showing relevant dimensions.

**National Instrument FieldPoint I/O-system
(connected to PC with RS-232 running LabView)**

**Input of 7 Thermocouples, 2
Pressure Gauges, and Cell Voltage**

**Controlled Power-Output for
Heating Tape and Catridge Heater**

Agilent 3000
Micro GC

Bypass flow
8 locations on both
anode and cathode

**H2
TANK**

**N2
TANK**

**CO2
TANK**

**O2
TANK**

**N2
TANK**

**AIR
TANK**

|	
Water - Trap	**Rotormeter / Flowmeter**
Heating Tape	**LynnTech Humidifier (mass- and temperature controlled)**
Catridge Heater	
Valve	**Thermocouple**
Pressure Sensor	**Data Direction**

**Figure 2.** Schematic of the experimental test stand and control system.

Figure 3. Time varying performance at 0.4, 0.6, and 0.8 V while mass distribution measurements were taken, indicating little effect of measurement on cell performance.
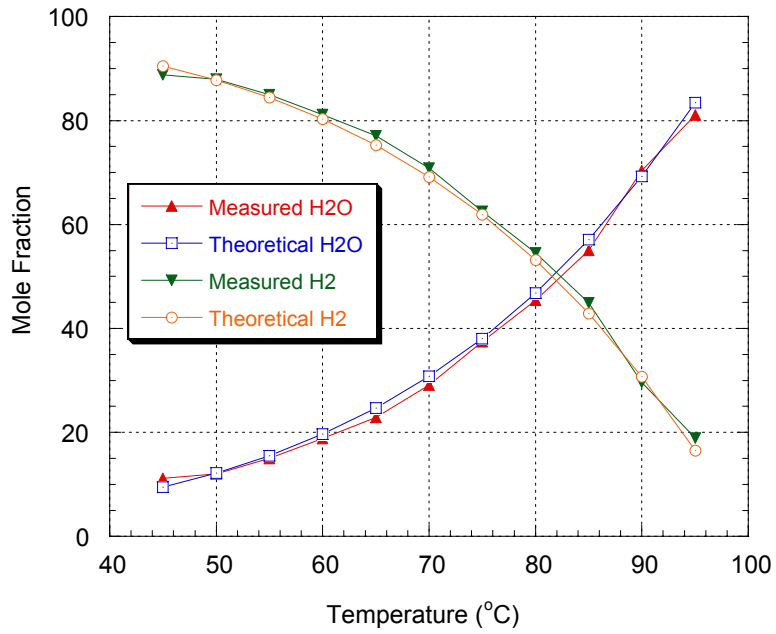
Figure 4. Comparison between measured and theoretical water vapor and hydrogen concentrations measured with GC with baseline value at 50 °C. The humidifier bottle was at 1.1 atm pressure.
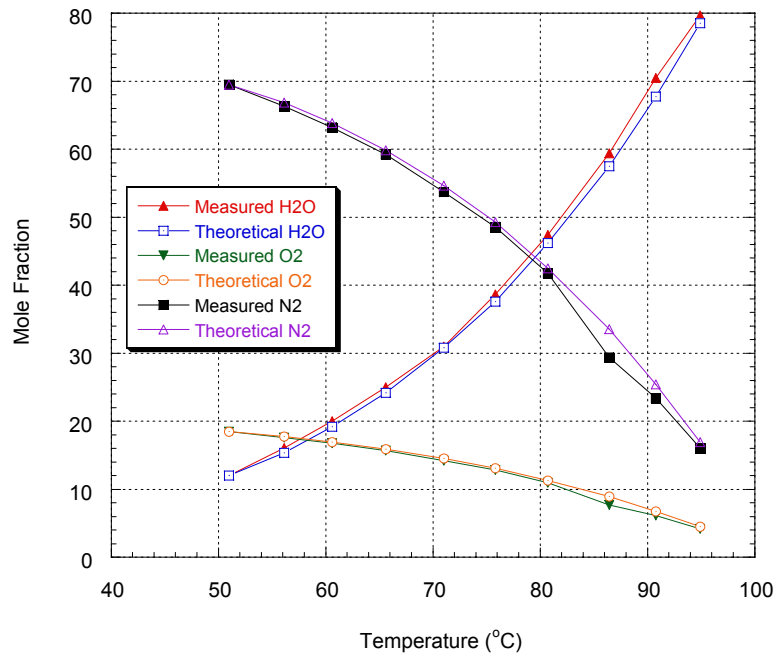
Figure 5. Comparison between measured and theoretical water vapor, nitrogen and oxygen concentrations measured with GC with baseline value at 50 °C. The humidifier bottle was at 1.1 atm pressure.
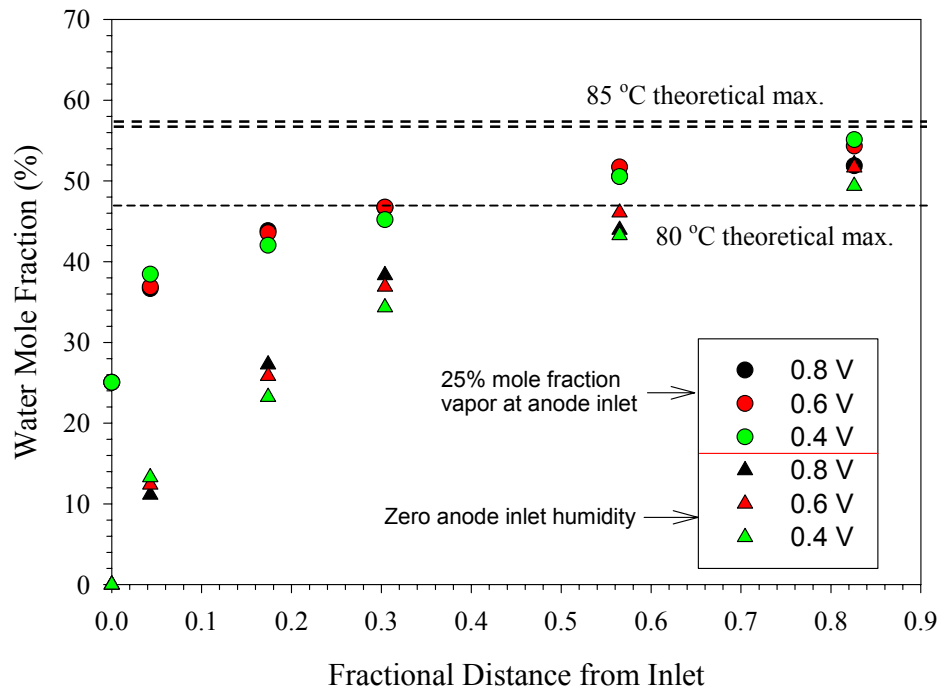
Figure 6. Measured water distribution as a function of fractional distance from anode inlet for partially, and non-humidified anode conditions. Test conditions: exit pressure A/C = 1 atm, 100% RH @ 80°C air cathode, 100% or 0% RH @ 65°C neat H_2 anode ξ_c = 2.5 @ 0.7 A/cm2 ξ_a = 1.0 @ 0.7 A/cm^2

Table 1. Baseline operating conditions.

Parameter	Value	Units
Electrolyte	Nafion 112	NA
Gas diffusion layer	ELAT® (De Nora North America) anode and cathode	NA
Catalyst loading (carbon supported)	0.5	mg/cm^2
Cell temperature	80	^{o}C
Anode inlet temperature	90	^{o}C
Cathode inlet temperature	80	^{o}C
Anode and cathode pressure	0.1	MPa
Cathode humidification	100% at 80°C	NA
Anode gas	Ultra high purity H$_2$ (>99.999 %)	NA
Cathode gas	Commercial air (79% N$_2$, 21% O$_2$)	NA